Tribological Behavior and Wear Mechanisms of TiN/TiCN/TiN Multilayer Coatings

Y.L. Su and W.H. Kao

(Submitted 21 April 1998; in revised form 19 May 1998)

This work employs the PVD process to deposit coatings of single layer TiN, binary layer TiN/TiCN, multilayer TiN\Ti\TiN, and sequenced TiN\TiCN\TiN multilayer coatings with variable individual TiN-layer and TiCN-layer thicknesses on tungsten carbide disks and inserts.

Also investigated are the fracture mechanisms and the influence of sequence and thickness of these coatings on cylinder-on-disk, line-contact wear mode and ball-on-disk, point-contact wear mode through SRV reciprocating wear tests. Actual milling tests identify wear performance.

Experimental results indicate that the coating with a total thickness of 7 μm and layer sequence TiN/TiCN/TiN exhibits good wear resistance on SRV wear test and milling test. The thickest multilayer TiN/Ti/TiN coating, although having the highest hardness, has the worst wear resistance for all tests. Notably zero-wear performance was observed for all coating disks under cutting fluid lubricated condition due to the transferred layers formed between the contact interface.

Keywords milling test, multilayer coatings, reciprocating wear, zero-wear

1. Introduction

Ceramic coatings are used extensively not only to fulfill the requirement of enhanced wear resistance for many applications of surface engineering, but also to enhance the service life of working tools and machine parts. For example, TiN is an extensively used coating in industrial applications (Ref 1, 2). Having become the standard use for cutting tools, forming tools, and machine parts for many years, this coating serves as a protective layer for tools due to its wear and corrosion resistance. Bull and Jones (Ref 3) studied multilayer coatings in the TiN system, demonstrating the excellent performance of compositionally and structurally modulated coatings in the system over the conventional single-layer titanium nitride coating in tribological applications.

TiCN is renowned for its better oxidation resistance and hot hardness than TiC (Ref 4-6). O. Knotek et al. (Ref 7) indicated that the merits of TiCN-coated carbide insert over other coatings such as TiN-coated inserts include its superior friction behavior in contact with steel and the high thermal transmission coefficient of the coating. D'Errico and Chiara (Ref 8) investigated the binary layer TiN/TiCN on ceramic inserts by a cathode arc deposition, indicating that the tool life was increased during dry force milling.

The researches of multilayer coatings in Ref 9 to 13 reveal not only their superior performance over comparable single-layer coatings, but also the attractive properties of different materials which they contain in a single protective layer. In fact, some multicomponent and multilayer coatings have already been found to be commercially usable, such as TiN/TiC/TiN (Ref 14) produced by the "high temperature" chemical vapor deposition (CVD) method. According to Leyland et al. (Ref 15), first generation coatings, such as TiN, are already widely used, whereas second generation coatings, such as TiCN and TiN, are highly promising for certain "niche" wear applications.

Leyland et al. also envisaged a potential growth market for third generation coatings, that is, the multicomponent and multilayer systems.

In light of above developments, this work uses the physical vapor deposition (PVD) method to produce TiN, TiN/TiCN, TiN/Ti/TiN, and a series of TiN/TiCN/TiN multilayer coatings with different coating sequences and thicknesses (Table 2). Also investigated herein is a series of tribological performances and fracture mechanisms of coatings on wear test and actual milling cutting. The extent to which coating sequences and thickness of TiN/TiCN/TiN multilayer coating influence wear character is examined. In addition, wear tests are performed under both dry and lubricated conditions; end milling tests are carried out under dry cutting condition as well. The

Y.L .Su and **W.H. Kao,** Department of Mechanical Engineering, National Cheng Kung University, Tainan, Taiwan.

Table 1 Nominal chemical compositions of the specimens

	Composition, wt%								
Specimens	**Fe**	**C**	**Si**	**Mn**	**P**	**S**	**Ni**	**Cu**	**Cr**
1045	bal	0.46	0.24	0.75	0.02	0.01	0.06	0.05	0.21
52100	bal	1.03	0.22	0.31	0.01	0.01	0.07	0.06	1.39

most appropriate multilayer coating for wear resistance is determined after the tests.

2. Experimental Details

2.1 Specimen Preparation and Coating Deposition

Coating layers were deposited on tungsten carbide (WC) bulk disks and WC inserts using the HC 1000, multi-arc PVD (MAPVD) system (Hauzer Techno Coatings, Venlo, Holland).

The materials of upper specimens for SRV test were AISI 1045 (cylinder) and AISI 52100 (ball) steels, whereas the material of the lower specimen was WC bulk disk. Table 1 lists the chemical compositions of 1045 and 52100 steels. A WC bulk disk is a powder metallurgy sintered part containing 6 wt% Co. The average size of the WC particle was ~0.5 μm. The fully mixed powders of WC and Co were compressed to a density of 14.73 cm^{-3}, followed by presintering at 600 to 1000 °C for 30 min; the powders were then sintered in a vacuum for two to three hours at 1450 to 1500 °C (Ref 16). Then, the WC specimen was mechanically polished to a roughness of $R_a \doteq 0.008$ μm, ultrasonically cleaned in acetone, and maintained in an electric dryer to prevent its surface from becoming polluted again.

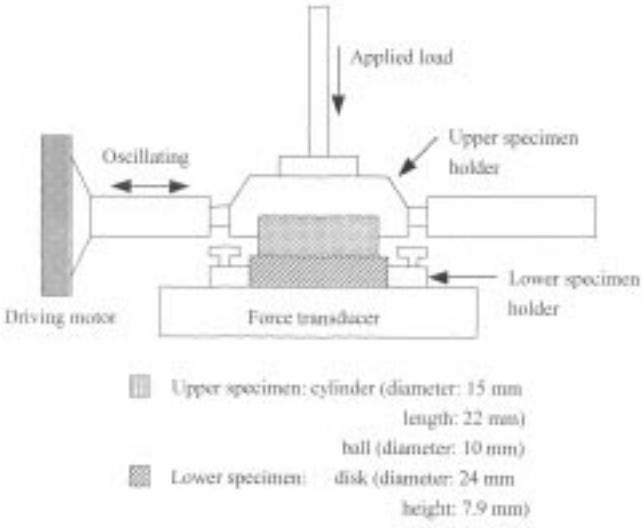

Fig. 1 SRV wear test machine

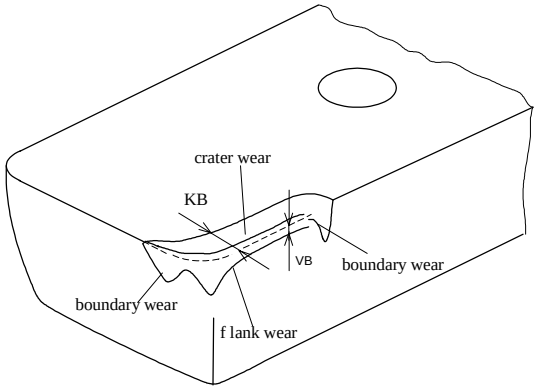

Fig. 2 Wear profile of milling tool

The R_a value of uncoated WC insert was ~0.16 μm; the surface of the insert was not polished prior to deposition to avoid changing the tool geometry.

The construction and sequence for multilayer coatings from substrate to top are TiN/TiCN/TiN, TiN/TiCN/TiN/TiCN/TiN, TiN/Ti/TiN/Ti/TiN, TiN/TiCN, and TiN as shown in Table 2, which were all deposited on substrates of WC bulk disk and inserts. Next, an interface layer of Ti about 0.1 μm thick was deposited between the substrate and the TiN layer to enhance the adhesion in this work (Ref 17, 18). Table 3 displays the process and parameters of deposition. Case 1 in Table 2 is a graded process coating. Partial pressure of CH_4 gradually increased from 0 to 4×10^{-3} mbar, and partial pressure of N_2 gradually decreased from 1×10^{-2} to 6×10^{-3} mbar. The chamber total press was 1×10^{-2} mbar.

The cylinder specimens were directly cut off from a milled round AISI 1045 steel and mechanically polished to a roughness of $R_a \approx 0.32$. The 52100 steel balls were commercial products, conventionally used in ball bearings. All the specimens were fabricated to a shape deemed appropriate for the SRV holder.

2.2 Hardness Tests

The hardness of the coating specimens was measured using a Vickers microhardness tester (Matsuzawa MXF70) under a load of 100 gf and 50 gf. Notably, the measured hardness is a mixture of the top layer, the medi-layers, and the substrate.

Table 2 Constructions and deposition sequences for multilayer coating

Case No.	Coating layers and sequences	Thickness
1	3 μm TiN + 2 μm TiCN + 2 μm TiN (graded)	7.0
2	3 μm TiN + 1 μm TiCN + 3 μm TiN	7.0
3	3 μm TiN + 2 μm TiCN + 2 μm TiN	7.0
4	2 μm TiN + 0.5 μm TiCN + 2 μm TiN + 0.5 μm TiCN + 2 μm TiN	7.0
5	2 μm TiN + 0.1 μm Ti + 2 μm TiN + 0.1 μm Ti + μm TiN	7.2
6	2 μm TiN + 0.1 μm Ti + 2 μm TiN + 0.1 μm Ti + μm TiN + 0.1 μm Ti + 3 μm TiN	9.3
7	3.5 μm TiN + 3.5 μm TiCN	7.0
8	7 μm TiN	7.0
9	Uncoated	…

Table 3 Depositions parameters for the multilayer coatings

Parameters	Single and multilayer of TiN	TiN/TiCN
Partial pressure of CH_4, mbar	…	4×10^{-3}
Partial pressure of N_2, mbar	1×10^{-2}	6×10^{-3}
Chamber pressure, mbar	1×10^{-2}	1×10^{-2}
Bias voltage, V	120	120
Arc current, A	80	80
Chamber temperature, °C	400	400
Evaporation temperature, °C	400	400
Evaporation rate, μm/h	4	4

2.3 Wear Test

Wear tests were performed using an oscillation, friction, and wear (SRV) reciprocating sliding machine (Optimal, Germany), as depicted in Fig. 1. The configuration of the SRV test machine consists of a fixed lower specimen supporter and a replaceable upper specimen holder. The upper specimen can be a ball or a cylinder block, depending on the holder type, while the lower specimen is a disk. Figure 1 displays the dimensions of the test specimens and a schematic diagram of the experimental setup.

The arrangement of a ball and a cylinder block mated with a disk formed a ball-on-disk point contact wear mode and a cylinder-on-disk line contact wear mode, respectively. The tests were performed at room temperature and atmospheric pressure. The relative humidity of the laboratory was about 45 to 55%. In addition, a constant 1 mm stroke, 100 N normal load, a 24 min test duration (144 m slide distance), and a 50 Hz frequency were employed.

The lubricants used in this study included HD-150 (Chinese Petroleum Co.) and water-based cutting fluid (CF). HD-150 possesses a kinematic viscosity of 138.9 cSt at 40 °C and 14.4 cSt at 100 °C, which contains sulfur and chlorine to form a sustainability of high pressure. The water-based cutting fluid contains neither sulfur nor chlorine; it has a specific gravity of 1.018 at 15 °C. The pH value of the 1 to 20 solution (diluted with water for application) ranges from 8.9 to ~9.2.

The maximum depth of wear scars on a lower test contacted disk was taken using a surface profilometer (Kosake SE30H, Japan) with a precision of ±0.005 μm at a magnification of $\times 10^6$.

All the tests were performed twice, and three different measurements were taken from each pass of the tests. Then, each of the six measurements from the same tests were averaged and all shown as the measurement results in this work.

2.4 Milling Test

The machining center (MCV-610AP, Leadwell; Taiwan) was used to perform this experiment. The tool holder was a Sandvik commercial product, No. U-MAX R215.44-32A-15C, with a diameter of 32 mm and four slots. The indexical WC inserts No. R215.44-15T308-15C-AAM, with ISO P30 application area, are also commercially available by Sandvik. An assembly of the tool holder and the WC insert produced a milling tool having the geometrical configuration of 0° radial rake angle, 5° axial rake angle, 11° clearance angle, 74° corner angle, and 0.8 mm noise radius.

In this experiment, a single-tooth laboratory cutting was used for the milling tests. The workpiece material was AISI 1045 steel cubic with a dimension of 90 mm × 90 mm × 90 mm and a bulk hardness of ~HB182. The cutting parameters were 0.1 mm/tooth feed rate, 120 m/min cutting speed, 1.5 mm depth of cut, and 90° engaged angle. The total volume of steel being cut out was 14.58×10^4 mm^3. No cutting fluid was added throughout the experiment.

Figure 2 illustrates the wear form of end mill cutters on milling test. The flank wear on the cutter was measured after each pass. Two cuttings were tested for each pass.

To precisely measure the width of the flank wear, a special fixture was manufactured to maintain the flank face horizontal.

2.5 Wear Surface Observation

A scanning electron microscope (SEM) was used to observe the worn surface of the multilayer coatings. Wavelength dispersive spectrometry (WDS) and energy dispersive spectrometry (EDS) were also used to determine the fracture mechanism.

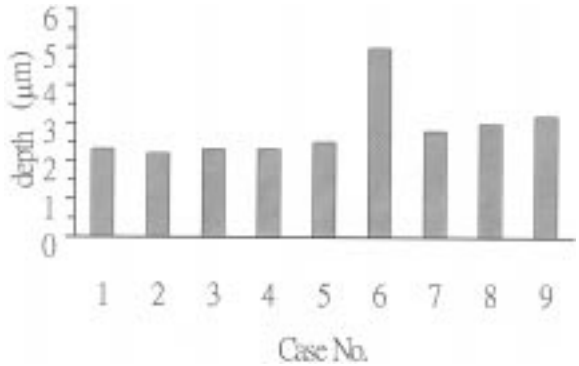

Fig. 3 The depth of wear scar on coating disks under dry condition (cylinder on disk)

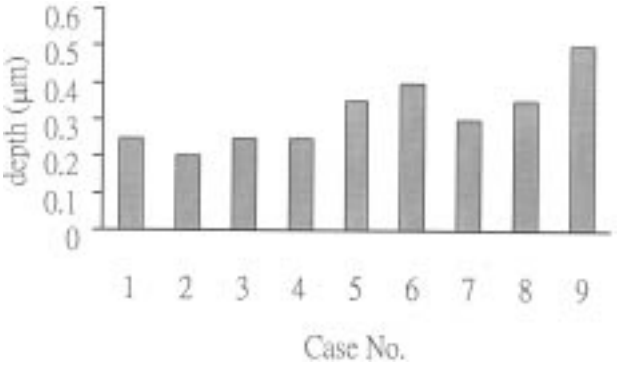

Fig. 4 The depth of wear scar on coating disks under HD-150 lubricated condition (ball on disk)

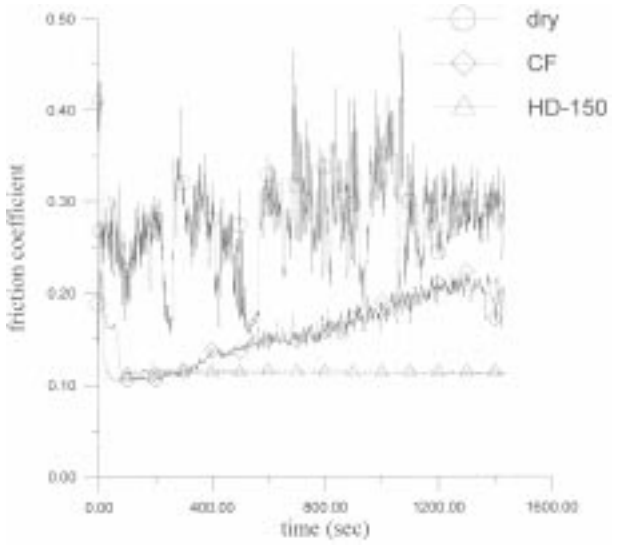

Fig. 5 Curve of friction coefficient during dry, cutting fluid (CF) and HD-150 lubricated conditions wear test

3. Results and Discussion

3.1 The Influences of Wear Type and Friction Trace under Dry and Lubricated Conditions on SRV Wear Test

Figures 3 and 4 summarize the different results of depth measured from wear scars on the coating disk under dry (cylinder-on-disk, line-contact wear mode) and HD-150 lubricated (ball-on-disk, point-contact wear mode) conditions, respectively. According to the figures, cases 6 and 9 have the deepest scars at either condition. The wear conditions can be classified into two groups according to wear resistance. Group 1 includes cases 1, 2, 3, and 4, in which the variable individual thickness of TiN, TiCN layers in the multilayer coatings (sequenced TiN/TiCN/TiN) are not influences of the wear resistance. Group 2 includes multilayers of TiN/Ti/TiN (cases 5 and 6), binary layer (case 7), single layer (case 8), and uncoated (case 9) disks, which all have a poor wear resistance. The friction coefficient was continuously recorded during the tests. Figure 5 summarizes typical results of dry and lubricated conditions. The friction trace displayed that a large fluctuation and multiple seizures shown by the (spike on the trace) occurred under the dry condition for coating disk against steel cylinder (cylinder-on-disk, line-contact wear mode). In addition, much noise was also induced during the wear test. Figure 6(a) presents the typical wear scars and original areas of multilayer coating surface. Figure 6(b) shows a magnification of Fig. 6(a), indicating that the worn surface was covered with red-brown oxide materials.

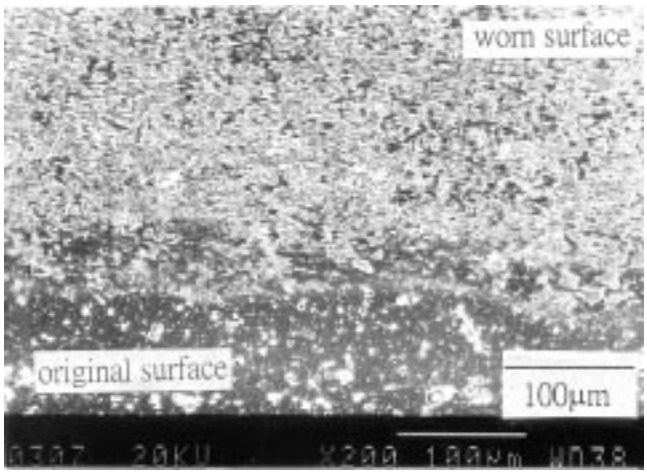

(a)

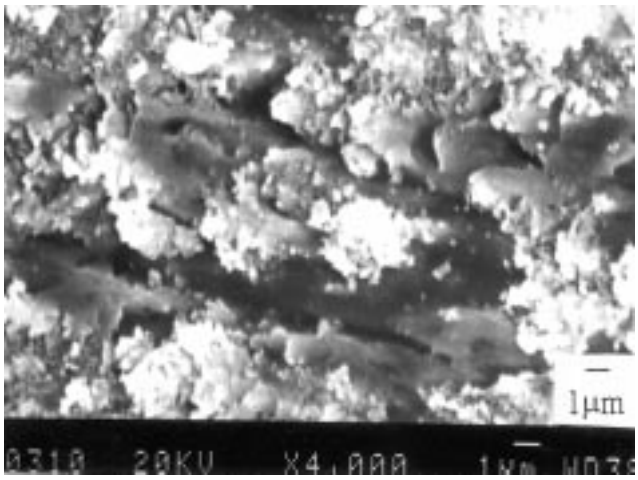

(b)

Fig. 6 (a) Typical original and worn surface of a coating disk under dry condition (cylinder on disk). (b) Magnified worn-surface micrograph of (a)

On the other hand, the typical friction trace displays a smooth curve under the HD-150 lubricated condition for coating disk against steel ball (ball-on-disk, point-contact wear mode), as shown in Fig. 5. This typical worn surface is local light rubbing and polish. As Fig. 7 shows, the rubbing behavior in this case is extremely mild, and this rubbing surface is attributed to the breakdown of lubrication, whether fluid-film or boundary. Therefore, results obtained from such a smooth curve of friction coefficient and less wear should be attributed to the lubricant on cooling and lubrication.

The typical friction trace reveals a small fluctuation under the CF lubricated condition for coating disk against steel ball (ball-on-disk, point-contact wear mode), as shown in Fig. 5. This fluctuation is due to a transferred layer being formed from the tribochemical reaction of steel ball and to CF becoming a protective layer on the lower coating disk. The fact that friction behavior occurred between the protective film and the reciprocating sliding steel ball and induced a light rubbing trace on the protective layer as shown in Fig. 14(a) accounts for why no wear occurred upon the coating layer on the disk during the tests. The next section describes this performance.

3.2 The Zero-Wear Operation under Cutting Fluid Condition

The unique characteristic of wear performance carried out under CF lubricated conditions is a zero-wear operation for all coating disks (ball-on-disk, point-contact wear mode) except the uncoated WC substrate. Figures 8(a) to (d) display the typical SEM micrograph results on the transferred layers on the coating disk after test 15 s, 1 min, 5 min, and 24 min, respectively. The transferred layers were formed on the coating disk, as stated in section 3.1, when wear tests were operated initially,

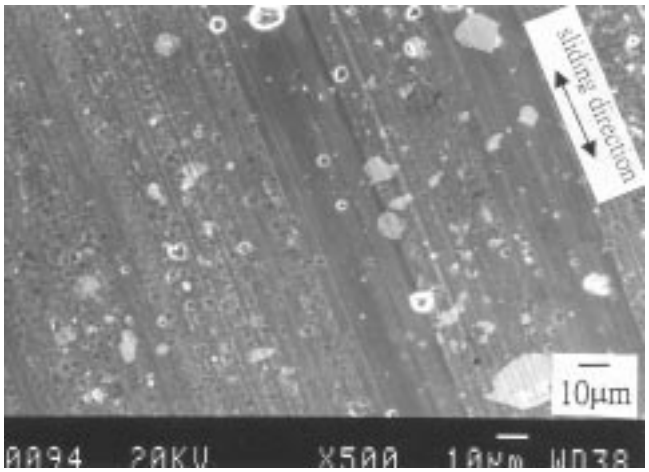

Fig. 7 Typical worn surface of coating disk against steel ball under HD-150 lubricated condition

as shown in Fig. 8(a). The transferred regions were then enlarged, as shown in Fig. 8(b) and (c). Finally, a protective layer was formed on each coating disk, as indicated in Fig. 8(d). For further analysis, the coating disks were leached in 100% HCl to remove the transferred layer after testing for 24 min; the polished feature can be observed, as shown in Fig. 8(e). Figure 8(f) presents a clearer magnified micrograph of (e). In contrast, the transferred layer phenomenon did not occur on an uncoated

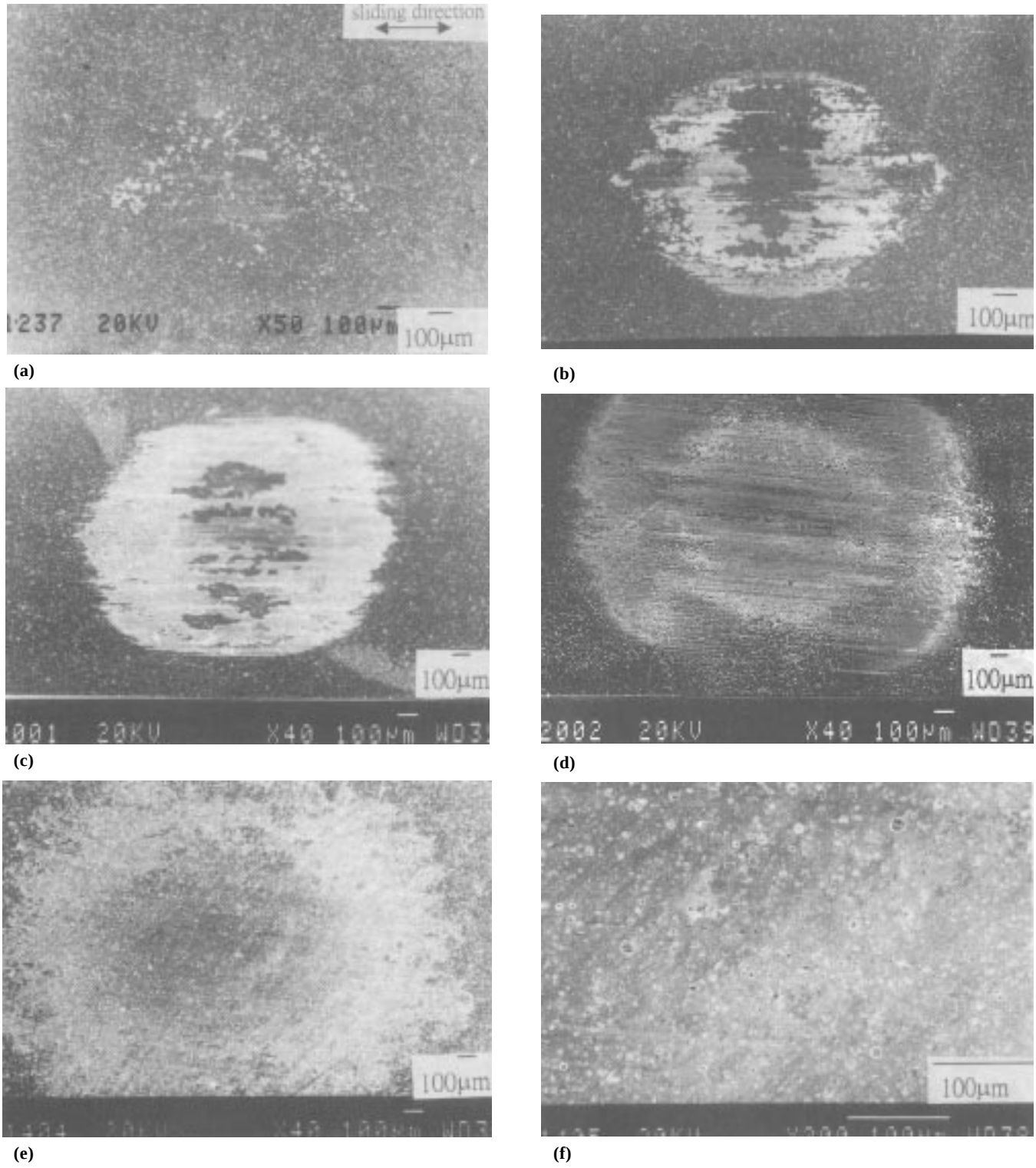

Fig. 8 Typical transferred layers of coating disk against steel ball under CF lubricated condition after test (a) 15 s, (b) 1 min, (c) 5 min, and (d) 24 min. (e) Polished feature of coating disk after test 24 min. (f) Magnification of (e) after leached in 100% HCl

WC substrate under a cutting fluid (ball-on-disk, point-contact wear mode). The worn surface was rubbing traces and adhesion of a few Fe elements, as shown in Fig. 9.

3.3 Adhesion Material and Wear-Scar Measurement Depth

This work also examines how an adhesion material produced by tribochemical reaction influences measurement depth of the deepest wear scar on the coating disks under dry condition (cylinder-on-disk, line-contact wear mode). The disks were leached in 100% HCl to remove the adhesion materials after the wear test. The wear scars on the coating disks before and after leaching in HCl were compared. Figures 10(a), (b), and (c) display the typical worn surface of coating disks against 1045 steel cylinder under dry condition, EDS analysis of Fig 10(a), and profile crossing wear scars of Fig. 10(a), respectively, before the disks leached in 100% HCl. Figure 10(b)

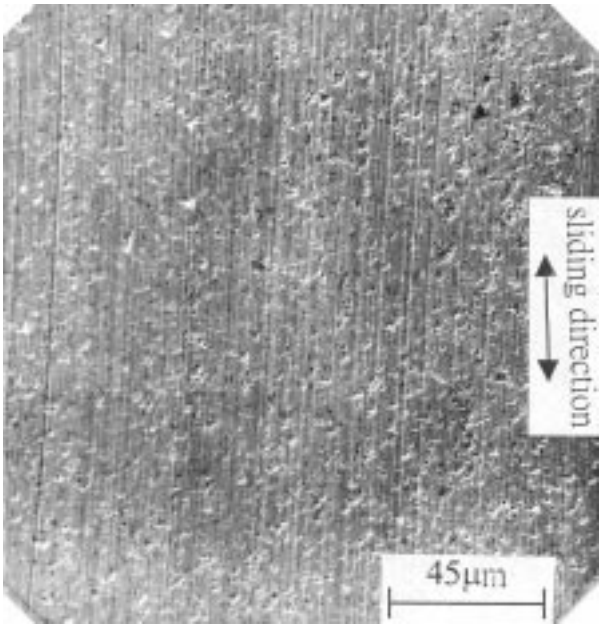

(a)

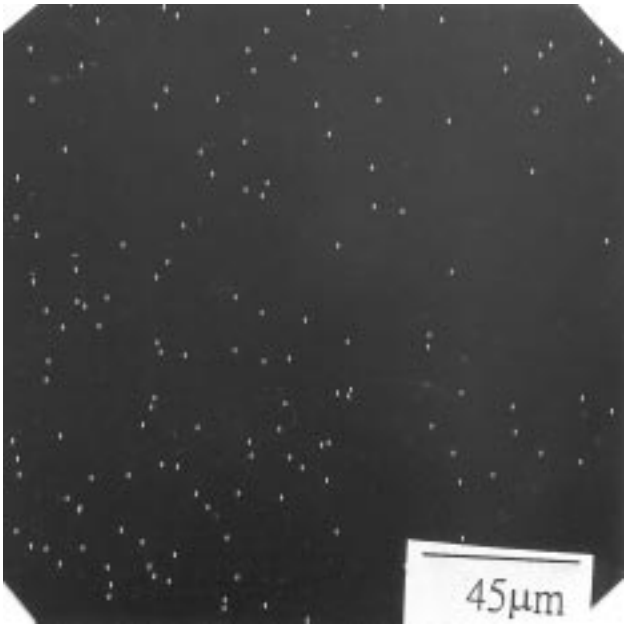

(b)

Fig. 9 (a) Wear scar of WC substrate against steel ball under cutting fluid lubricated condition and (b) corresponding Fe x-ray mapping of (a)

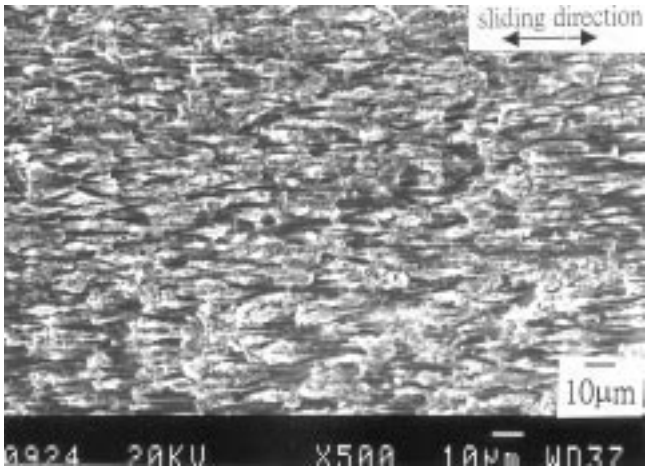

(a)

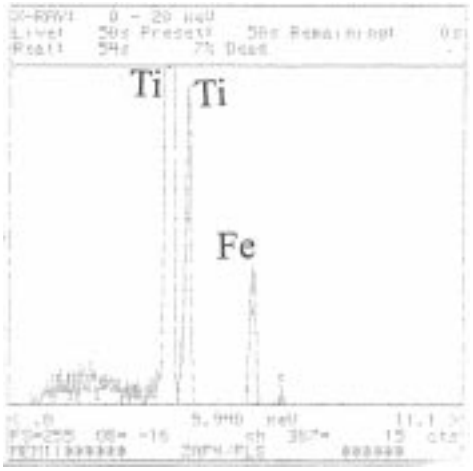

(b)

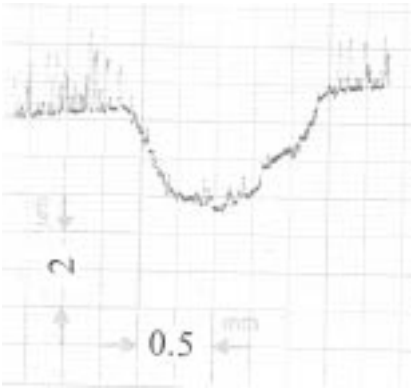

(c)

Fig. 10 (a) Typical wear scar of coating disks against steel cylinder under dry condition before leached in 100% HCl. (b) Corresponding EDS analysis of (a). (c) Typical profile crossing wear scar of (a)

reveals that iron oxide adhered to the worn surface and induced a rough curve and a few spikes on the profile, as shown in Fig. 10(c).

Figures 11(a), (b), and (c) display the typical worn surface of coating disks against 1045 steel cylinder under dry condition, EDS analysis of Fig 11(a), and profile crossing worn scar of Fig 11(a), respectively, after the disks were leached in 100% HCl. Figure 11(b) indicates that the major adhesion of iron oxide was eliminated from the worn surface. Comparing the profiles of Fig. 10(c) and Fig. 11(c) reveals that the deepest depth of the wear scars is the same, indicating that the measurement depth of the wear scars is convincing.

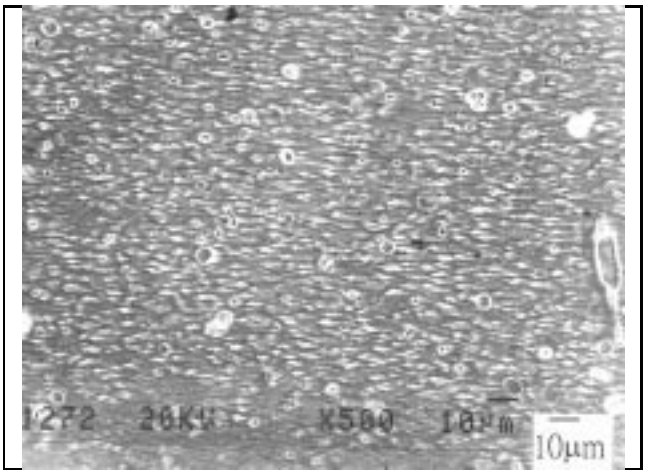

(a)

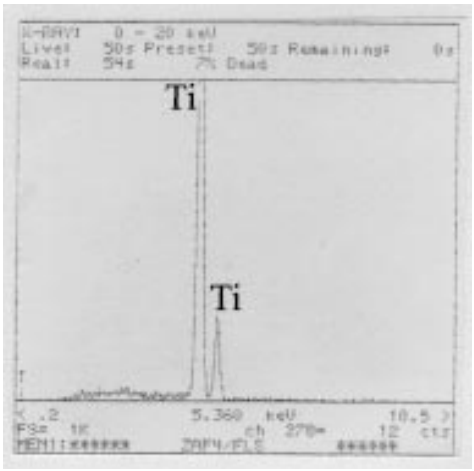

(b)

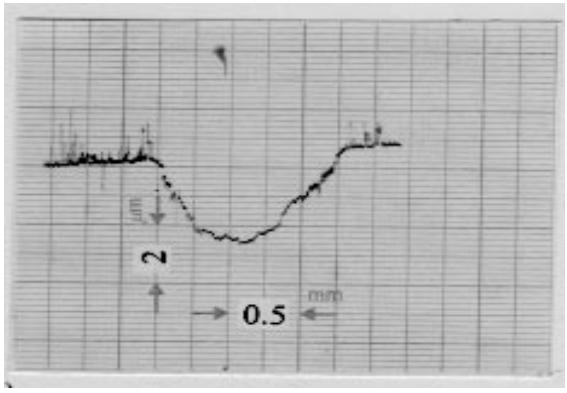

(c)

Fig. 11 (a) Typical wear scar of coating disks against steel cylinder under dry condition after leached in 100% HCl. (b) Corresponding EDS analysis of (a). (c) Typical profile crossing wear scar of (a)

3.4 Milling Results

Under the same milling conditions in this test, the flank wears of end mill cutter are illustrated in Fig. 12. The multilayer coating with 7 μm thickness and sequence of TiN/TiCN/TiN (cases 1, 2, 3, and 4) possessed the optimum wear resistance. The binary layer coating TiN/TiCN (case 7) is better than the single-layer TiN (case 8) coating, while the single-layer TiN coating is better than the uncoated tool (case 9). Furthermore, the same result was found on the SRV test. In addition, of all coatings, the multilayer coating TiN/Ti/TiN (case 6) had the worst wear resistance. Moreover, all the coated tools have a better wear resistance than the uncoated tools.

3.5 Relationship between the Wear Resistance against the Coating Thickness and the Deposition Sequence

Table 4 summarizes the experimental results from the SRV wear test and milling tests, revealing the influence of deposition sequences and coating thickness of the multilayer against the wear resistance. The coating with sequence of TiN/TiCN/TiN and thickness of 7 μm (cases 1, 2, 3, and 4) has a better wear resistance. Therefore, the coatings with TiN/TiCN/TiN sequence (cases 1, 2, 3, and 4) are the most appropriate coatings against wear.

Table 4 also displays the hardness of the specimens with various combinations of the coating layers under the same WC substrate. The coating hardness is obviously increased with an increase of coating thickness. However, increasing the hardness of a specimen does not always indicate a better wear resistance since the residual stress that increased with coating thickness yields a poor adhesion of the coating. According to Arai et al. (Ref 19) , the adhesion strength of the coating layers can be estimated from the radial and lateral cracks surrounding the indentation. Figures 13(a) and (b) display the SEM mi-

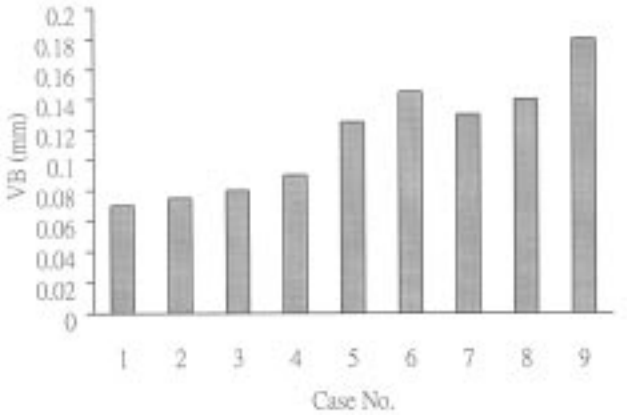

Fig. 12 Flank wear on milling cutters under milling test

crographs of indentations in cases 1 and 6, respectively. The surface fracture (Fig. 13a) was found to be a few cracks and slight coating detachment around the indentation, indicating that the coating has a good adhesion in case 1. In contrast, Fig. 13(b) shows that there was severe and large area spall around the indentation, indicating that the coating is highly brittle and has poor adhesion in case 6. Therefore, the coating layer in case 1 has a better adhesion strength than that in case 6. The failure type in other cases is similar in appearance as shown in Fig. 13(a), case 1.

Table 4 Surface microhardness, depth of worn scar and flank wear on the coating specimens

Case No.	Coating thickness, μm	Microhardness, HV 50 g	Microhardness, HV 100 g	Depth of wear scar, μm dry (cylinder on disk)	Depth of wear scar, μm CF (ball on disk)	Depth of wear scar, μm HD-150 (ball on disk)	Flank wear, VB (milling cutter) mm
1	7.0	2320	2100	2.3	0	0.25	0.060
2	7.0	2270	2200	2.2	0	0.20	0.075
3	7.0	2360	2290	2.3	0	0.25	0.085
4	7.0	2640	2450	2.3	0	0.25	0.090
5	7.2	2490	2340	2.5	0	0.35	0.125
6	9.3	3150	2770	5.0	0	0.40	0.145
7	7.0	2830	2670	2.8	0	0.30	0.130
8	7.0	2660	2500	3.0	0	0.35	0.140
9	…	1774	…	3.2	0.3	0.50	0.180

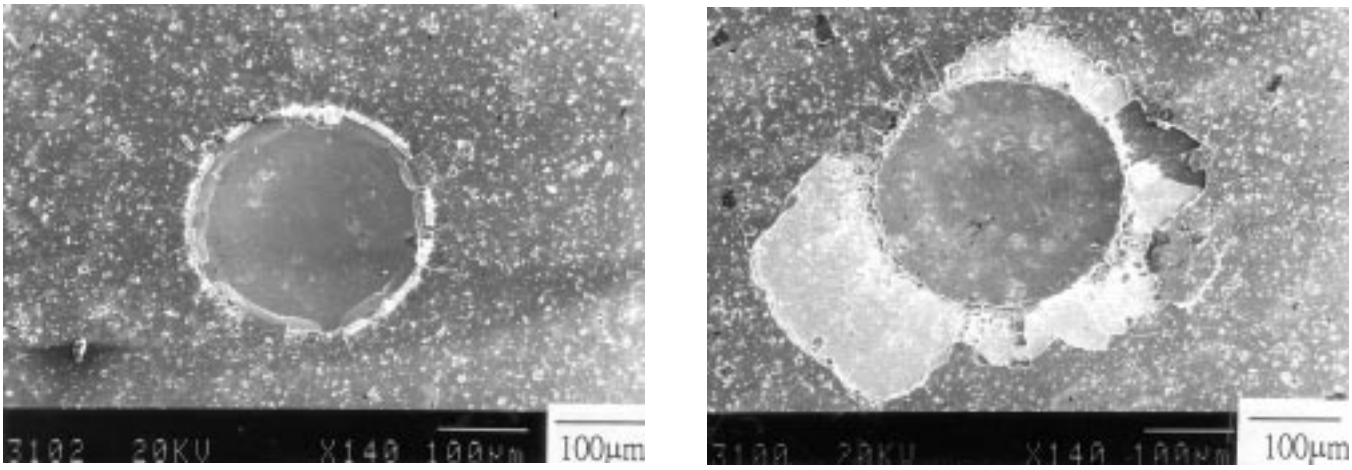

(a) **(b)**

Fig. 13 Failure types of (a) case 1 and (b) case 6 coatings after indentations

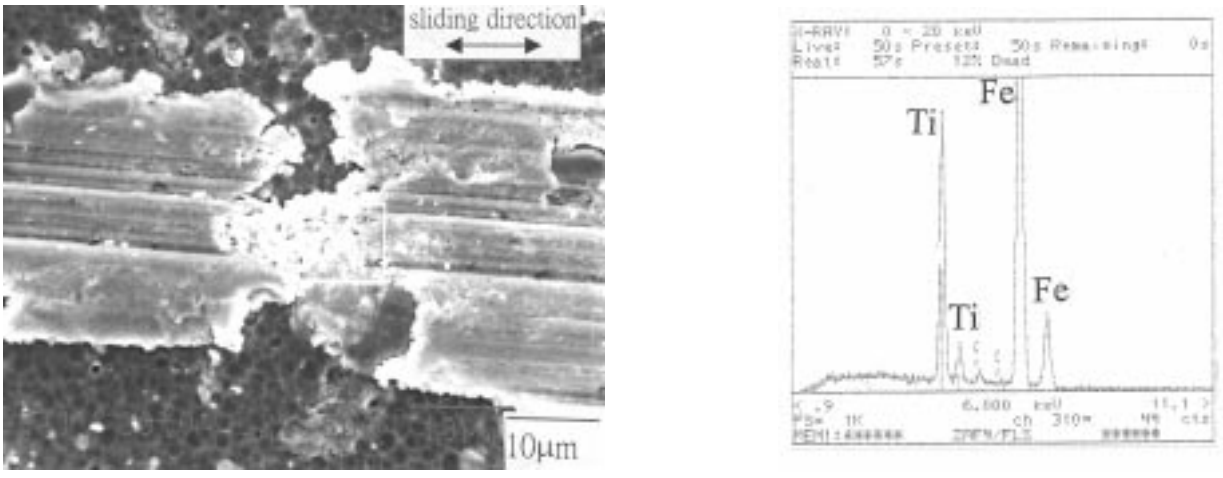

(a) **(b)**

Fig. 14 (a) Transferred layer and particles on coating disk after testing 15 s. (b) Corresponding EDS analysis of (a)

Consequently, the multilayer in case 6 is the worst case of all the multilayers under wear and milling tests, although it has the highest hardness of all.

4. Wear Mechanisms

4.1 SRV Wear Test

The wear behavior occurs between the protective layer on the coating disk and the reciprocating steel ball under CF lubricated condition. Therefore, the zero-wear is substantiated by this operation on coating disk.

The overall protective layer process is described as follows: (1) Small particles of debris, produced from the tribochemical reaction of steel ball and CF, form between the coating disk and the reciprocating steel ball. (2) Tribochemical reaction accompanied with reciprocating motion joins the small particles together, forming the transferred layer. Figure 14(a) presents the transferred layer formation by connecting the small particles of debris locally marked after testing 15 s. Figure 14(b) displays the corresponding EDS analysis of the transferred layer and particles, indicating that its major element is Fe element from the steel ball. (3) The protective layer forms from the gradually enlarged material of the transferred layer.

The typical worn feature between coating disks and steel cylinder under dry condition is the typical tribochemical and adhesion reaction, as shown in Fig. 15. In Fig. 15(a), the conglomeration adhesion to the worn coating surface is observed. Figure 15(b) indicates that the same conglomeration back transferred to the steel cylinder. The debris was created by tribochemical reaction between the wear pair. The debris color is reddish brown, indicating that the major material of debris is oxide Fe_2O_3 (Ref 20, 21), accompanied by a few adhesion materials from the coating surface. Figures 16 (a) and (b) illustrate the micrographs of debris and corresponding EDS analysis, respectively, revealing that the major tribochemical reaction is Fe from the steel cylinder. A mixture of adhesion and oxidation was the major wear process.

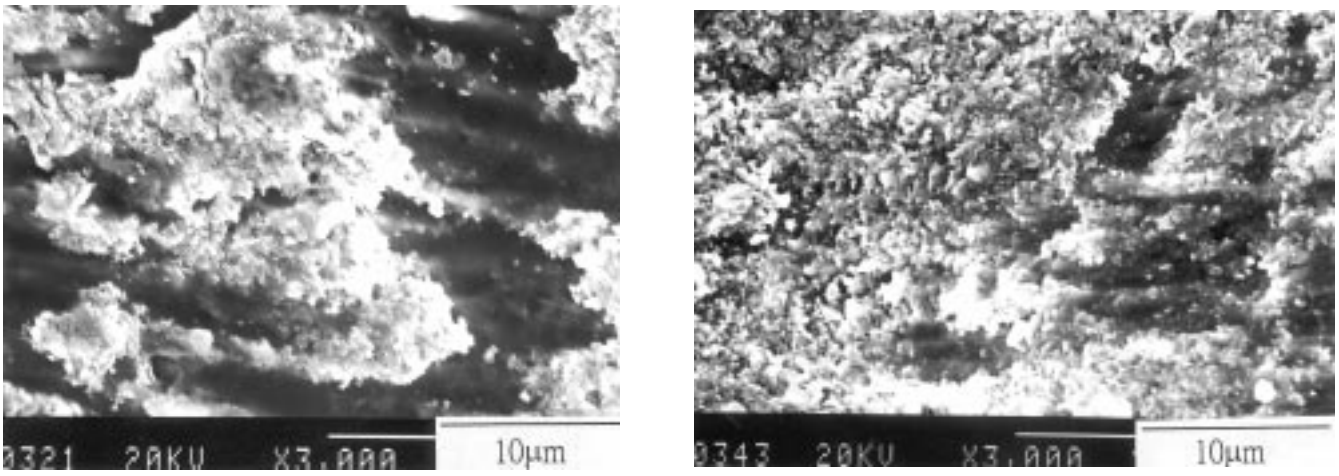

(a) **(b)**

Fig. 15 Typical worn surfaces created in dry condition after wear test on (a) coating disk and (b) 1045 steel cylinder

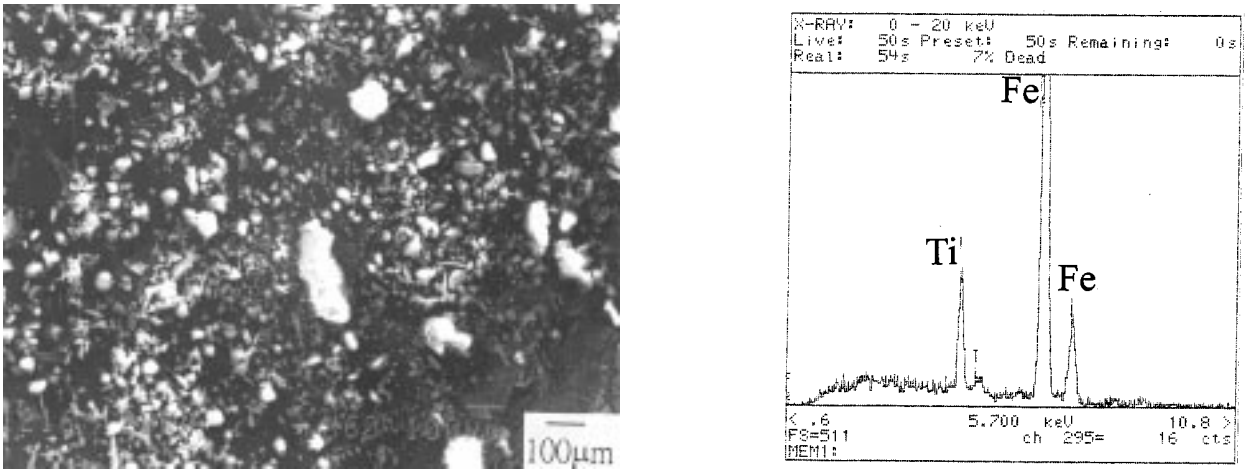

(a) **(b)**

Fig. 16 (a)Typical wear debris of coating disk against 1045 steel cylinder under dry condition and (b) corresponding EDS analysis of (a)

4.2 Milling Test

Figure 17 depicts the typical configuration difference in the wear process between the coated and uncoated WC inserts. The crater wear processes do not occur on the coated tools, in which the flank wear revealed the gradient wear profile for coated WC inserts, while the uncoated WC insert had the precipitously worn profile. Therefore, the wear of the coated tool that occurred only on the cutting edge at the beginning was then enlarged. Those results could be attributed to the excellent wear resistance of the coating layers.

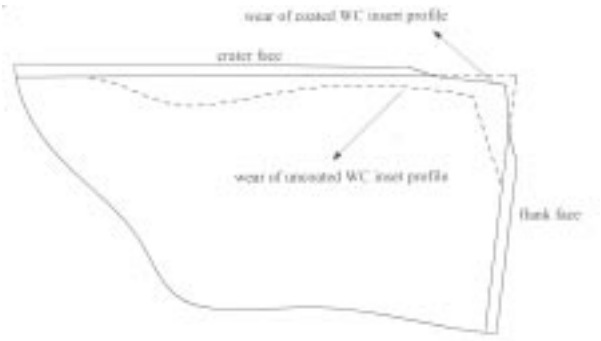

Fig. 17 Schematic representation for the wear configuration of multilayer coated and uncoated WC insert

The adhesive wear on the flank of binary-layer TiN/TiCN coated insert (case 7) is primarily a fracture mechanism, as shown in Fig. 18(a) and (b), which corresponds to the mapping of Fe in (a). Figure 18(a) also includes some location coating on the flank, removed by the adhered process and gradually deepening to the WC substrate.

On the other hand, the fracture mechanism attributed primarily to adhesive wear can induce cracks on a single-layer TiN coating. Figure 19 indicates that the flake and cracks fracture are on the flank of a single-layer coated insert (case 8). For further analysis, the coated WC inserts (case 8) were leached in 100% HCl to remove the adhered layer. The thermal crack nucleation at aperture can be observed in a coating layer, and the crack propagates by joining the cracks between aperture and

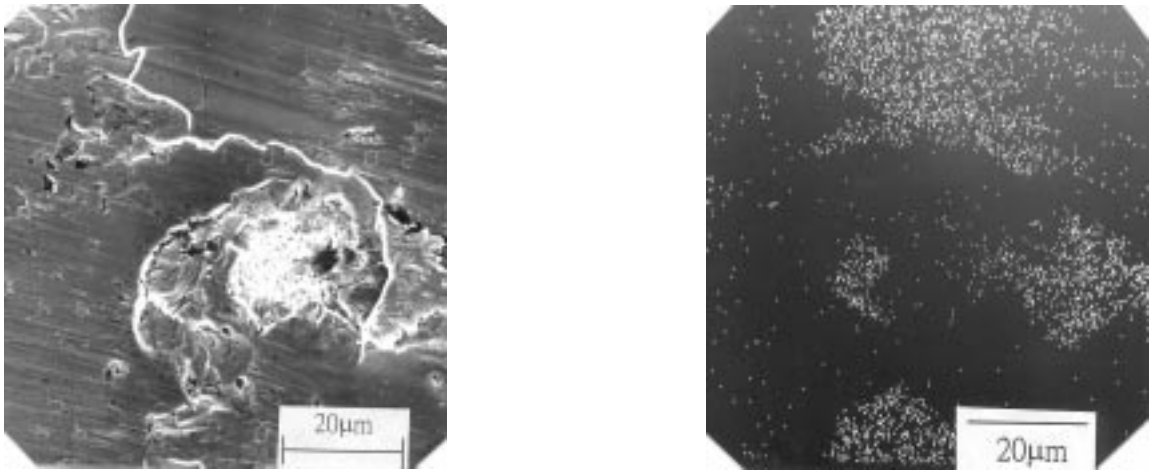

(a) **(b)**

Fig. 18 (a) Adhesion wear of binary layer coated insert and (b) corresponding x-ray mapping of Fe in (a)

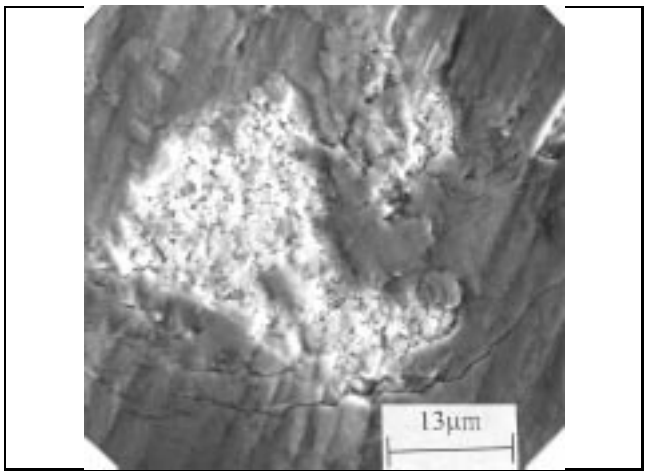

Fig. 19 Flank wear of single layer coated insert is flake and cracks fracture

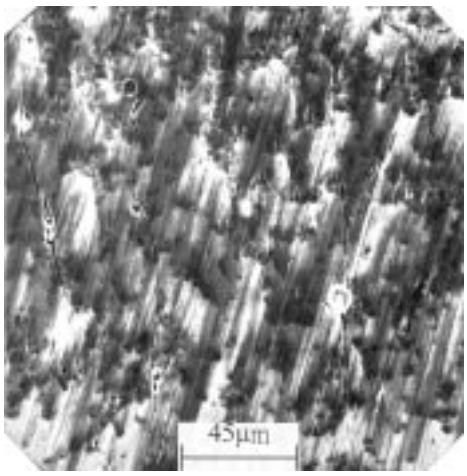

Fig. 20 A mechanism of the thermal crack nucleation at the aperture in the coating layer

aperture, as shown in Fig. 20. The fracture mechanism of a single-layer (case 8) insert is shown in Fig. 21(a), which reveals thermal cracks propagated along the direction perpendicular to the cutting edge. Figure 21(b) shows fatigue cracks perpendicular to the thermal cracks of Fig. 21(a). When these two kinds of cracks react alternately, the coating layer is induced to flake and breakdown. In contrast, the extent and amount of thermal and fatigue cracks are much less for multilayer films and binary-layer film than for single-layer TiN film. Furthermore, the multilayer films have a higher resistance than single-layer films in terms of the enlargement of the cracks caused by the fatigue and thermal action.

5. Conclusions

Based on the results in this work, we can conclude:

- Wear experiments indicate that among all the multilayer coatings, 7 μm- thick layers with sequence TiN/TiCN/TiN have the optimum wear resistance for the reciprocating wear test.
- Although the thickest multilayer TiN/Ti/TiN coating has the highest hardness, the worst wear resistance occurs under dry reciprocating sliding. This is attributed to the embrittlement and poor adhesion of the coating layer.
- Milling test results indicate that multilayer TiN/TiCN/TiN coatings have better wear resistance than the binary-layer TiN/TiCN and the single-layer TiN coating. This enhanced resistance is attributed to the thermal and fatigue cracks reduction for multilayer coatings.
- The primary wear mechanism, for binary-layer TiN/TiCN coated and multilayer TiN/TiCN/TiN coated milling cutters, is adhesion wear. However, for a single-layer TiN coated milling cutter, thermal and fatigue cracks accelerate the wear process.
- The transferred layer forms a protective film on the coating disks, resulting in zero-wear operation under cutting fluid lubricated condition.

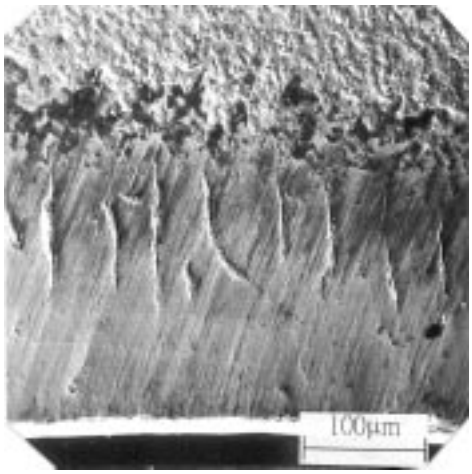

(a)

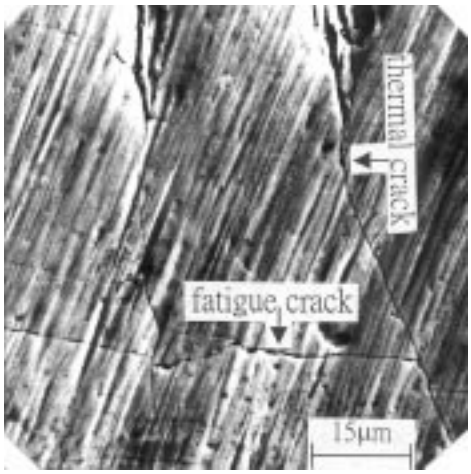

(b)

Fig. 21 Cracks of single layer coated insert on flank wear with (a) the thermal cracks and (b) the fatigue and thermal cracks perpendicular after leaching in 100% HCl

Acknowledgments

The authors would like to thank the National Science Council under contract number NSC-86-2216-E-006-046 and also the Cho Chang Tsung Foundation of Education for their financial support. Special thanks to C.T. Wu for his deposition.

References

1. E. Bergman, H. Kaufmann, R. Schmid, R. Schmid, and J. Vogel, Ion-plated Titanium Carbonitride Films, *Surf. Coat. Technol.*, Vol 42, 1990, p 237-251
2. H. Holleck, Material Selection for Hard Coatings, *J. Vac. Sci. Technol. A*, Vol 4 (No. 6), 1986, p 2661-2669
3. S.J. Bull and A.M. Jones, Multilayer Coatings for Improved Performance, *Surf. Coat. Technol.*, Vol 78, 1996, p 173-184
4. M. Tamura and H. Kubo, Deposition and Annealing Effect on Ti(C,N) Coatings, *Surf. Coat. Technol.*, Vol 49, 1991, p 275-278
5. H.O. Pierson, A Review of the CVD of the Refractory Compounds of Titanium—A Unique Family of Coatings, *Mater. Manuf. Process.*, Vol 8 (No. 4), 1993, p 519-534
6. O. Knotek, Ti(CN) Coating Using the Arc Process, *Surf. Coat. Technol.*, Vol 46, 1991, p 39-46
7. O. Knotek, F. Loffler, and G. Kramer, Deposition, Properties and Performance Behaviour of Carbide and Carbonnitride PVD Coatings, *Surf. Coat. Technol.*, Vol 61, 1993, p 320-325
8. G.E. D'Errico and R. Chiara, PVD Coating of Cermet Inserts for Milling Applications, *Surf. Coat. Technol.*, Vol 86-87, 1996, p 735-738
9. E. Vancoille, J.P. Celis, and J.R. Roos, Tribological and Structural Characterization of a Physical Vapour Deposition TiC/Ti(CN)/TiN Multilayer, *Tribol. Int.*, Vol 26 (No. 2), 1993, p 115-119
10. U. Helmersson, S. Todorova, L.C. Markert, S.A. Barnett, J.E. Sundgern, and J. Geene, Growth of Single-Crystal TiN/VN Strained-Layer Superlattices with Extremely High Mechanical Hardness, *J. Appl. Phys.*, Vol 62, 1987, p 481-484
11. J.E. Sundgern, J. Birch, G. Hakansson, L. Hultman, and U. Helmersson, Growth, Structural Characterization and Properties of Hard and Wear-Protective Layered Materials, *Thin Solid Films*, Vol 193/194, 1990, p 818-831
12. H. Holleck and H. Schulz, Advanced Layer Material Constitution, *Thin Solid Films*, Vol 153, 1987, p 11-17
13. T. Cselle and A. Barimani, Today's Applications and Future Development of Coating for Drills and Rotating Cutting Tools, *Surf. Coat. Technol.*, Vol 76-77, 1995, p 712-718

14. "Metalworking Products—Turning Insert Program," Sandvik Coromant, Sweden, 1989

15. A. Leyland, K.S. Francy, and A. Matthews, Plasma Nitriding in a Low Pressure Triode Discharge to Provide Improvements in Adhesion and Load Support for Wear Resistant Coatings, *Surf. Eng.*, Vol 7, 1991, p 207-215

16. R.M. German, *Powder Metallurgy Science*, p 241-296, MPIF, Princeton, 1994

17. C. Subramanian and K.H. Strafford, Review of Multicomponent and Multilayer Coating for Tribological Applications, *Wear*, Vol 165, 1993, p 85-95

18. K.A. Pischow, L. Eriksson, E. Harju, A.S. Korhonen, and E.O. Ristolainen, The Influence of Titanium Interlayers on the Adhesion of PVD TiN Coating on Oxidized Stainless Steel Substrates, *Surf. Coat. Technol.*, Vol 58, 1993, p 163-172

19. T. Arai, H. Fujita, and M. Watanabe, Valuation of Adhesion Strength of Thin Hard Coatings, *Thin Solid Films*, Vol 154, 1987, p 387-401

20. T.F.J. Quinn, Oxidational Wear, *Wear*, Vol 18, 1971, p 413-419

21. T.F.J. Quinn, The Role of Oxide Films in the Friction and Wear Behavior of Metals, *Tribology Series 7*, Elsevier, Amsterdam, 1982, p 579